

Fermi-ball in a multicomponent dark matter framework and its gravitational wave signatures

Nabarun Chakrabarty*

*Department of Physics, Siksha Bhavana, Visva-Bharati,
Santiniketan, West Bengal 731235, India*

Indrani Chakraborty†

*Department of Physics and Material Science and Engineering,
Jaypee Institute of Information Technology, A-10,
Sector-62, Noida 201307, Uttar Pradesh, India*

Himadri Roy‡

*Institute of Particle Physics and Key Laboratory of Quark and Lepton Physics (MOE),
Central China Normal University, Wuhan, Hubei 430079, China*

Abstract

It has been known that under-abundant dark matter density of an inert doublet can be replenished by an additional dark matter component, say, a fermion. We find that such a scenario can lead to the formation of stable Fermi-balls through coexisting minima of the finite temperature scalar potential. More importantly, we demonstrate that the Fermi-balls contribute sizeably to the dark matter relic density. In addition, the aforesaid coexisting minima open up the possibility of a first-order phase transition. This, in turn, triggers emission of gravitational waves that can be tested at the proposed BBO and U-DECIGO detectors. Therefore, the present study becomes a concrete setup to embed Fermi-balls in a realistic two-component dark matter model, and, to test the same using gravitational wave signatures.

*Electronic address: chakrabartynabarun@gmail.com

†Electronic address: indrani300888@gmail.com

‡Electronic address: himadri027roy@gmail.com

I. INTRODUCTION

Various experimental findings such as galaxy rotation curves and gravitational lensing point towards the existence of cosmologically stable dark matter (DM) [1, 2]. While the nature of DM is under investigation, its amount in the universe is precisely known from the latest measurements by the PLANCK satellite [3]. Conceiving DM as an elementary particle calls for extending the Standard Model (SM) since there is no such candidate in the latter [4]. In fact, it has been hypothesised that DM is a weakly interacting massive particle (WIMP) [5] whose interaction strengths to the particles in the thermal bath is in the *weak* ball-park. However, it is this sizeable interaction strengths that has cornered most minimal WIMP scenarios in view of the null results from direct detection experiments [6–9].

The lack of precise information on DM quantum numbers leads to the possibility that DM consists of more than one type of particle (a partial list is [10–24]). Multi-particle DM frameworks are interesting since they predict DM-DM interaction. And while the processes driven by such interaction can contribute to the DM relic density, they have no role in DM-nucleon scattering thereby keeping the direct detection rates unchanged.

There is a growing interest in studying the possibility of a first order phase transition (FOPT), and, the consequential gravitational wave (GW) spectrum in dark matter models [25–49]. FOPTs involve co-existing minima, typically dubbed as the false and the true vacua, of the free energy functional. And [50] introduced the idea that a fermionic DM candidate can get trapped inside the false vacuum and form compact macroscopic DM candidates called Fermi-balls. The conditions that must be satisfied here are (a) a substantial mass gap of the fermion between false and true vacua compared to the phase transition temperature, (b) asymmetry in the number densities of the fermion and its antiparticle, and (c) the fermion must carry a conserved global charge Q . More details can be found in [50] and are skipped here for brevity.

In this study, we look at the possibility of stable Fermi-ball formation in a multicomponent DM setup. The inert scalar doublet scenario (see [51–61] and the references therein), a popular WIMP setup, is extended by adding a fermion χ and a scalar S , both gauge singlets. The fermion interacts with the rest of the fields through the scalar S . Such a scenario was considered in [62]. The fermion χ is endowed with a global $U(1)_Q$ and is thus cosmologically stable. We revisit the calculation of relic density of the resulting two-component DM setup. It is reconfirmed that χ can replenish the relic density in parameter regions where the standalone inert doublet falls under-abundant, i.e., the inert doublet *desert region*. Therefore, we focus mainly on the desert region in this study. Investigating the thermally corrected scalar potential along the direction of S leads to coexisting vacua in the parameter space of interest. We also compute the ensuing GW spectrum for representative benchmarks and

comment on their observability in the proposed satellite based GW detectors. Apart from these, we report stable Fermi-ball formation in the desert region and compute their contribution to the observed DM abundance. In all, this study realises Fermi-balls in an ultraviolet (UV)-complete DM model.

This paper is organized as follows. We theoretical set up is introduced in section II and the ensuing multicomponent DM phenomenology is elucidated in section III. In section IV, we shed light on the possibility of an FOPT concomitant with the DM aspects of the scenario. The GW spectrum arising out of such an FOPT is also quantified. In addition, we investigate the formation of stable Fermi-balls in the relevant parameter space of the model and estimate the contribution of Fermi-balls to the observed DM relic density. We summarise in section V. Important formulae are relegated to the Appendix.

II. THEORETICAL SETUP

In addition to the SM-like scalar doublet Φ , the scalar sector of the present setup comprises an additional doublet η and a gauge singlet S . Of these, Φ and S respectively pick up vacuum expectation values (VEVs) v and v_S . On the other hand, an odd \mathbb{Z}_2 parity is assigned to η in view of its DM candidacy thereby preventing the same to pick up a VEV. The particle content of the scalar multiplets is given below.

$$\Phi = \begin{pmatrix} G^+ \\ \frac{1}{\sqrt{2}}(v + h_0 + iG_0) \end{pmatrix}, \quad \eta = \begin{pmatrix} \eta^+ \\ \frac{1}{\sqrt{2}}(\eta_R + i\eta_I) \end{pmatrix}, \quad S = v_S + s_0 \quad (1)$$

With the \mathbb{Z}_2 ensuring stability on a cosmological time scale, the neutral inert scalars η_R and η_I become potential DM candidates. The scalar potential consistent with the gauge and \mathbb{Z}_2 symmetries reads.

$$\begin{aligned} V(H, \eta, S) = & -m_\Phi^2 \Phi^\dagger \Phi + m_\eta^2 \eta^\dagger \eta - \frac{1}{2} m_S^2 S^2 - \frac{\mu_S}{3} S^3 + \lambda_1 (\Phi^\dagger \Phi)^2 + \lambda_2 (\eta^\dagger \eta)^2 \\ & + \lambda_3 (\Phi^\dagger \Phi) (\eta^\dagger \eta) + \lambda_4 (\Phi^\dagger \eta) (\eta^\dagger \Phi) + \left[\frac{1}{2} \lambda_5 (\eta^\dagger \Phi)^2 + h.c. \right] \\ & + \frac{1}{2} \lambda_6 \Phi^\dagger \Phi S^2 + \frac{1}{2} \lambda_7 \eta^\dagger \eta S^2 + \frac{1}{4} \lambda_8 S^4. \end{aligned} \quad (2)$$

It is demanded that $m_\Phi^2 > 0$, $m_\eta^2 > 0$, $m_S^2 > 0$ in order to ensure the said configuration of the VEVs of the neutral scalars in this setup. The tadpole conditions lead to

$$m_\Phi^2 = \lambda_1 v^2 + \frac{1}{2} \lambda_6 v_S^2, \quad (3a)$$

$$m_S^2 = -\mu_S v_S + \lambda_8 v_S^2 + \frac{1}{2} \lambda_6 v^2. \quad (3b)$$

The \mathbb{Z}_2 symmetry forbids η to mix with the other multiplets and thus the inert scalars are mass eigenstates with masses M_{η_R}, M_{η_I} and M_{η^+} as expressed below.

$$M_{\eta_R}^2 = m_\eta^2 + \frac{1}{2}(\lambda_3 + \lambda_4 + \lambda_5)v^2 + \frac{1}{2}\lambda_7 v_S^2, \quad (4a)$$

$$M_{\eta_I}^2 = m_\eta^2 + \frac{1}{2}(\lambda_3 + \lambda_4 - \lambda_5)v^2 + \frac{1}{2}\lambda_7 v_S^2, \quad (4b)$$

$$M_{\eta^+}^2 = m_\eta^2 + \frac{1}{2}\lambda_3 v^2 + \frac{1}{2}\lambda_7 v_S^2, \quad (4c)$$

On the other hand, as shown below, an h_0 - s_0 mixing does take place controlled by an angle θ . It leads to the mass eigenstates h and H .

$$\begin{pmatrix} h_0 \\ s_0 \end{pmatrix} = \begin{pmatrix} \cos\theta & \sin\theta \\ -\sin\theta & \cos\theta \end{pmatrix} \begin{pmatrix} h \\ H \end{pmatrix} \quad (5)$$

One defines $\lambda_L = \lambda_3 + \lambda_4 + \lambda_5$ in motivated from the fact that the $\eta_R - \eta_I - h$ interaction strength in the $s_\theta \rightarrow 0$ limit is $-\lambda_L v$. With this, we deem the following parameters to be independent while describing the scalar sector: $\{M_h, M_H, M_{\eta_R}, M_{\eta_I}, M_{\eta^+}, \mu_S, v_S, \lambda_L, \lambda_2, \lambda_7, s_\theta\}$. The various quartic couplings and m_η are expressible in terms of the independent parameters as

$$m_\eta^2 = M_{\eta_R}^2 - \frac{1}{2}\lambda_L v^2 - \frac{1}{2}\lambda_7 v_S^2, \quad (6a)$$

$$\lambda_1 = \frac{M_h^2 c_\theta^2 + M_H^2 s_\theta^2}{2v^2}, \quad (6b)$$

$$\lambda_3 = \lambda_L + \frac{2(M_{\eta^+}^2 - M_{\eta_R}^2)}{v^2}, \quad (6c)$$

$$\lambda_4 = \frac{(M_{\eta_R}^2 + M_{\eta_I}^2 - 2M_{\eta^+}^2)}{v^2}, \quad (6d)$$

$$\lambda_5 = \frac{(M_{\eta_R}^2 - M_{\eta_I}^2)}{v^2}, \quad (6e)$$

$$\lambda_6 = \frac{2(M_H^2 - M_h^2)s_\theta c_\theta}{vv_S}, \quad (6f)$$

$$\lambda_8 = \frac{M_h^2 s_\theta^2 + M_H^2 c_\theta^2}{2v_S^2} + \frac{\mu_S}{2v_S}. \quad (6g)$$

Further, an $SU(2)_L$ singlet Dirac fermion χ is introduced that is charged under a global $U(1)_Q$. This symmetry is imposed with Fermi-ball formation in mind. Further, the same also makes χ a DM candidate by stabilising it cosmologically. The Lagrangian involving χ therefore reads

$$\mathcal{L}_Y = -m_\chi \bar{\chi}\chi - y_\chi \bar{\chi}\chi S. \quad (7)$$

We note that the symmetries of the setup permit an inclusion of a bare mass parameter m_χ . The physical mass of χ therefore becomes $M_\chi = m_\chi + y_\chi v_S$. We choose to describe the fermionic sector in terms of the independent parameters $\{M_\chi, y_\chi\}$.

III. DM PHENOMENOLOGY

The setup admits two DM candidates, i.e., the CP-even inert scalar η_R and the fermion χ , by virtue of the \mathbb{Z}_2 and $U(1)_Q$ symmetries. It is mentioned that the only way χ interacts with the SM is via the scalar S . The relic abundance of χ is therefore largely dictated by its annihilations to SM particles and H , all imperatively s-channel processes mediated by h and H . As for η_R , the annihilation channels are (i) s-channel $\eta_R \eta_R \rightarrow SM SM$ processes mediated by h, H , (ii) t/u-channel $\eta_R \eta^\pm (\eta_I) \rightarrow V V$ processes mediated by $\eta^\pm (\eta_I)$ with $V = W^\pm Z$ as appropriate, and (iii) processes driven by the $\eta_R - \eta_R - h - h, \eta_R - \eta_R - h - H, \eta_R - \eta_R - H - H, \eta_R - \eta_R - V - V$ four-point interactions. Co-annihilation of η_R with the heavier inert scalars can also get triggered for small mass splittings thereby contributing to the relic density. In addition the $\chi\chi \leftrightarrow \eta_R\eta_R$ conversion processes can also play a prominent role when there are two dark sectors involved as in the present case.

The expressions for $\chi\chi \rightarrow \eta_R\eta_R, \eta_I\eta_I, \eta^+\eta^-$ annihilation cross-section are given below for the sake of completion.

$$\sigma_{\chi\chi \rightarrow \eta_R\eta_R} = \frac{1}{16\pi s} \sqrt{\frac{s - 4M_\chi^2}{s - 4M_{\eta_R}^2}} \left| \frac{y_{h\chi\chi} \lambda_{h\eta_R\eta_R}}{s - M_h^2 + iM_h\Gamma_h} + \frac{y_{H\chi\chi} \lambda_{H\eta_R\eta_R}}{s - M_H^2 + iM_H\Gamma_H} \right|^2 (s - 4M_\chi^2), \quad (8a)$$

$$\sigma_{\chi\chi \rightarrow \eta_I\eta_I} = \frac{1}{16\pi s} \sqrt{\frac{s - 4M_\chi^2}{s - 4M_{\eta_I}^2}} \left| \frac{y_{h\chi\chi} \lambda_{h\eta_I\eta_I}}{s - M_h^2 + iM_h\Gamma_h} + \frac{y_{H\chi\chi} \lambda_{H\eta_I\eta_I}}{s - M_H^2 + iM_H\Gamma_H} \right|^2 (s - 4M_\chi^2), \quad (8b)$$

$$\sigma_{\chi\chi \rightarrow \eta^+\eta^-} = \frac{1}{16\pi s} \sqrt{\frac{s - 4M_\chi^2}{s - 4M_{\eta^+}^2}} \left| \frac{y_{h\chi\chi} \lambda_{h\eta^+\eta^-}}{s - M_h^2 + iM_h\Gamma_h} + \frac{y_{H\chi\chi} \lambda_{H\eta^+\eta^-}}{s - M_H^2 + iM_H\Gamma_H} \right|^2 (s - 4M_\chi^2). \quad (8c)$$

The Yukawa and trilinear couplings appearing above are expressed in the Appendix. The thermal relics of χ and η_R are obtained by solving the coupled Boltzmann equations below. We define $x = \mu_{\text{red}}/T$, where μ_{red} denotes the reduced mass defined through $\mu_{\text{red}} = \frac{M_\chi M_{\eta_R}}{M_\chi + M_{\eta_R}}$.

$$\begin{aligned} \frac{dy_\chi}{dx} = & \frac{-1}{x^2} \left[\langle \sigma v_{\chi\chi \rightarrow \chi\chi} \rangle (y_\chi^2 - (y_\chi^{EQ})^2) + \langle \sigma v_{\chi\chi \rightarrow \eta_R\eta_R} \rangle \left(y_\chi^2 - \frac{(y_\chi^{EQ})^2}{(y_{\eta_R}^{EQ})^2} y_{\eta_R}^2 \right) \Theta(M_\chi - M_{\eta_R}) \right. \\ & \left. - \langle \sigma v_{\eta_R\eta_R \rightarrow \chi\chi} \rangle \left(y_{\eta_R}^2 - \frac{(y_{\eta_R}^{EQ})^2}{(y_\chi^{EQ})^2} y_\chi^2 \right) \Theta(M_{\eta_R} - M_\chi) \right] \end{aligned} \quad (9a)$$

$$\begin{aligned} \frac{dy_{\eta_R}}{dx} = & \frac{-1}{x^2} \left[\langle \sigma v_{\eta_R\eta_R \rightarrow \chi\chi} \rangle (y_{\eta_R}^2 - (y_{\eta_R}^{EQ})^2) + \langle \sigma v_{\eta_R\eta_R \rightarrow \chi\chi} \rangle \left(y_H^2 - \frac{(y_{\eta_R}^{EQ})^2}{(y_\chi^{EQ})^2} y_\chi^2 \right) \Theta(M_H - M_1) \right. \\ & \left. - \langle \sigma v_{\chi\chi \rightarrow \eta_R\eta_R} \rangle \left(y_\chi^2 - \frac{(y_\chi^{EQ})^2}{(y_{\eta_R}^{EQ})^2} y_{\eta_R}^2 \right) \Theta(M_\chi - M_{\eta_R}) \right]. \end{aligned} \quad (9b)$$

Here y_i ($i = \chi, \eta_R$) is related to the co-moving number density $Y_i = \frac{n_i}{s}$ (where n_i refers to DM density and s is entropy density) by $y_i = 0.264 M_{\text{Pl}} \sqrt{g_*} \mu Y_i$; similarly for equilibrium density, $y_i^{EQ} = 0.264 M_{\text{Pl}} \sqrt{g_*} \mu Y_i^{EQ}$, with equilibrium distributions (Y_i^{EQ}) have the form

$$Y_i^{EQ}(x) = 0.145 \frac{g}{g_*} x^{3/2} \left(\frac{m_i}{\mu} \right)^{3/2} e^{-x \left(\frac{m_i}{\mu} \right)}. \quad (10)$$

Here, $M_{\text{Pl}} = 1.22 \times 10^{19}$ GeV, $g_* = 106.75$ and m_i denotes M_χ and M_{η_R} . Further, X in eqn. 9 denotes the SM particles, η^\pm and η_I . This is because η^\pm is expected to be in equilibrium with the thermal plasma on account of electromagnetic interactions. Also, η_I being heavier than η_R can decay to η_R and SM fermions (f) via an off-shell $Z \rightarrow f\bar{f}$. Both η^+ and η_I thus remain in equilibrium with the thermal bath. The thermally averaged annihilation cross section, given by

$$\langle \sigma v \rangle = \frac{1}{8m_i^4 T K_2^2\left(\frac{m_i}{T}\right)} \int_{4m_i^2}^{\infty} \sigma(s - 4m_i^2) \sqrt{s} K_1\left(\frac{\sqrt{s}}{T}\right) ds \quad (11)$$

is evaluated at the freeze-out temperature T_f and denoted by $\langle \sigma v \rangle_f$. One notes that T_f is derived from the equality condition of DM interaction rate $\Gamma = n_{\text{DM}} \langle \sigma v \rangle$ with the rate of expansion of the universe $\bar{H}(T) \simeq \sqrt{\frac{\pi^2 g_*}{90}} \frac{T^2}{M_{\text{Pl}}}$. Further, $K_{1,2}(x)$ are the modified Bessel functions in eqn.(11).

It must be noted that the contribution to the Boltzmann equations coming from the DM-DM conversion depends on the mass hierarchy of DM particles. Thus the use of the Θ -function in the above equations. These coupled equations can be solved numerically to find the asymptotic abundance of the DM particles, $y_i \left(\frac{\mu_{\text{red}}}{m_i} x_\infty \right)$, which can be further used to express the contributions to relic density as

$$\Omega_i h^2 = \frac{854.45 \times 10^{-13} m_i}{\sqrt{g_*}} \frac{m_i}{\mu} y_i \left(\frac{\mu}{m_i} x_\infty \right), \quad (12a)$$

where x_∞ indicates an asymptotic value of x after the freeze-out. The index i stands for DM components in our scenario: χ, η_R . However, we use numerical techniques to solve for relic density of this two component model. The model is first implemented in LanHEP [64]. A compatible output was then fed into the publicly available tool micrOMEGAs4.3 (capable of handling multi-partite DM scenarios)[65] to compute the relic densities of χ and η_R .

In order to gain some insight on the relic density generation, we fix $v_S = M_H = \mu_S = 200$ GeV, $\mu_S = 50$ GeV, $\lambda_2 = \lambda_L = 0.01$, $\sin\theta = 5 \times 10^{-4}$ and plot the individual relic densities

¹ One is supposed to use g_{*s} in the above equations. However, $g_{*s} \simeq g_*$ holds for temperatures $\sim \mathcal{O}$ (GeV) or above[63].

versus M_χ for certain fixed values of M_{η_R} , y_χ and λ_7 . Fig.1 displays such plots corresponding to $M_{\eta_R} = 300$ GeV, $\lambda_7 = 1, 2$, $y_\chi = 0.5, 1, 2$. Resonance dips noted at $M_\chi = M_h/2$, $M_H/2$, and, the more the value of y_χ , the lesser is $\Omega_\chi h^2$. Both these observations are expected of the h, H -mediated s-channel amplitudes that are also proportional to y_χ . We find from Fig.1 that $\Omega_\chi h^2$ in the observed ballpark is obtained for $y_\chi \gtrsim 1$ for the values chosen for v_S , M_H and μ_S . A general feature is that $\Omega_\chi h^2$ starts increasing for $M_\chi > M_H$. A mild dependence on λ_7 is also noted owing to the $\chi\chi \leftrightarrow \eta_R\eta_R$ conversion amplitude being approximately proportional to λ_7 for small s_θ .

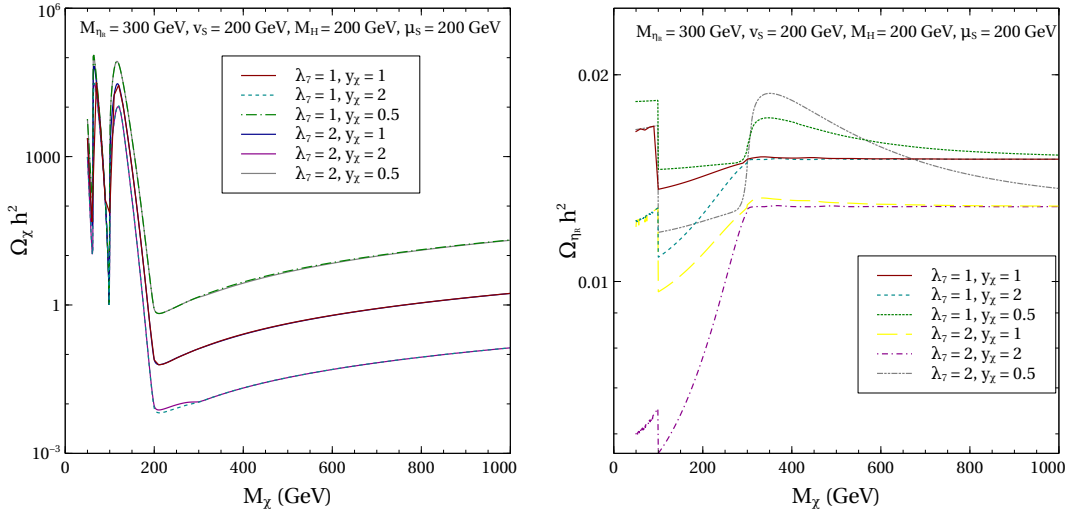


FIG. 1: Variation of $\Omega_\chi h^2$ (left) and $\Omega_{\eta_R} h^2$ (right) versus M_χ for $M_{\eta_R} = 300$ GeV. The color coding is explained in the legends.

The contribution of the inert doublet to the observed relic density is $\simeq 10\%$ in the desert region. In addition to the (co)annihilations processes for the standalone inert doublet model, $\eta_R\eta_R \rightarrow hH, HH$ become operative in the present setup. The sensitivity to λ_7 is seen to be higher in case of $\Omega_{\eta_R} h^2$. This is confirmed by the right plot of Fig.1. The individual relic densities for $M_{\eta_R} = 500$ GeV shown in Fig.2 also affirm the aforementioned observations.

Direct detection experiments such as LUX [66], PandaX-II [67] and Xenon-1T [68] look for DM-nucleon scatterings in terrestrial detectors. However, the non-observation of such processes has put stringent upper bounds on the corresponding cross sections. In our setup, both the DM candidates interact with the nucleons via t-channel processes mediated by h and H . The spin-independent direct detection (SI-DD) cross sections for η_R and χ respectively

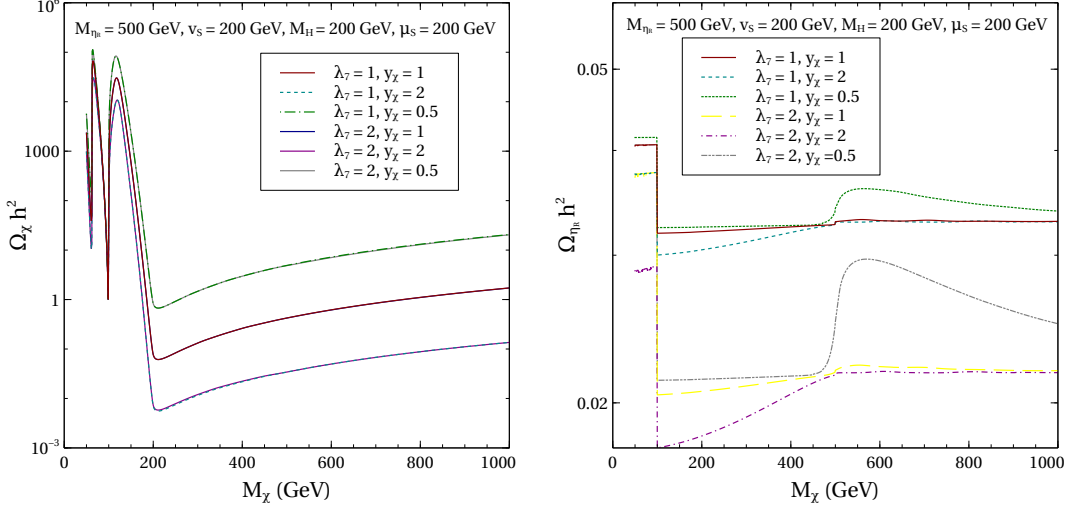


FIG. 2: Variation of $\Omega_\chi h^2$ (left) and $\Omega_{\eta_R} h^2$ (right) versus M_χ for $M_{\eta_R} = 500$ GeV. The color coding is explained in the legends.

are

$$\sigma_{\eta_R}^{SI} = \frac{\mu_{H,n}^2}{4\pi} \left[\frac{m_n f_n}{M_{\eta_R} v} \left(\frac{\lambda_{h\eta_R\eta_R}}{M_h^2} + \frac{\lambda_{H\eta_R\eta_R}}{M_H^2} \right) \right]^2. \quad (13a)$$

$$\sigma_\chi^{SI} = \sin 2\theta \frac{\mu_{N_1,n}^2}{4\pi} \left[\frac{y_\chi m_n f_n}{v} \left(\frac{1}{M_H^2} - \frac{1}{M_h^2} \right) \right]^2 \quad (13b)$$

where $\mu_{\eta_R,n} = m_n M_{\eta_R} / (m_n + M_{\eta_R})$, $\mu_{\chi,n} = m_n M_\chi / (m_n + M_\chi)$ are the DM-nucleon reduced masses and $f_n = 0.2837$ is the nucleon form factor [69]. In this two-component DM framework, the *effective* SI-DD cross sections relevant for each of the candidates can be expressed by the individual DM-nucleon cross-section scaled by the relative abundance of that particular component ($\Omega_i h^2$) in the observed DM relic density ($\Omega_{\text{obs}} h^2$). That is,

$$\sigma_{i,eff}^{SI} = \frac{\Omega_i h^2}{\Omega_{\text{obs}} h^2} \sigma_i^{SI}. \quad (14)$$

We adopt $\Omega_{\text{obs}} h^2 = 0.12$ here. It is ensured in the subsequent analysis that $\sigma_{\eta_R,eff}^{SI}$ and $\sigma_{\chi,eff}^{SI}$ respect the latest XENON-1T bounds. A more careful analysis for multi-particle DM direct search cross section can be performed by computing total recoil rate (see for instance, [13–16]), however the above procedure gives a correct order of magnitude estimate for individual components.

IV. DYNAMICS OF A FOPT

Since χ couples only to the scalar S prior to EWSB, the Fermi-ball dynamics is dictated by the thermal evolution of the vacuum expectation value $\langle S(T) \rangle$. Therefore, we examine

the scalar potential as a function of a background field ϕ in the direction of the scalar S . The tree level potential is straightforwardly found to be

$$V_0(\phi) = -\frac{1}{2}m_S^2\phi^2 - \frac{1}{3}\mu_S\phi^3 + \frac{1}{4}\lambda_8\phi^4. \quad (15)$$

Next, we quote the corresponding one-loop Coleman-Weinberg potential [70] in dimensional regularisation (DR). That is,

$$V_{\text{CW}}(\phi) = \frac{1}{64\pi^2} \sum_i n_i \left\{ M_i^4(\phi) \log\left(\frac{M_i^2(\phi)}{\mu^2}\right) - \frac{3}{2} \right\}. \quad (16)$$

Here, μ is the renormalisation scale encountered in dimensional regularisation (DR) and i runs over all particles interacting with S . The i th particle has n_i number of degrees of freedom, and, picks up a field dependent mass $M_i(\phi)$ in the process. One finds

$$n_{G^+} = n_{\eta^+} = 2, \quad n_{G_0} = n_{h_0} = n_{\eta_R} = n_{\eta_I} = 1, \quad n_\chi = -4. \quad (17)$$

The various field-dependent masses are expressed as

$$M_{G^+}^2(\phi) = M_{G_0}^2(\phi) = M_{h_0}^2(\phi) = -m_\Phi^2 + \frac{1}{2}\lambda_6\phi^2, \quad (18a)$$

$$M_{\eta^+}^2(\phi) = M_{\eta_I}^2(\phi) = M_{\eta_R}^2(\phi) = m_\eta^2 + \frac{1}{2}\lambda_7\phi^2, \quad (18b)$$

$$M_S^2(\phi) = -m_S^2 - 2\mu_S\phi + 3\lambda_8\phi^2, \quad (18c)$$

$$M_\chi^2(\phi) = (m_f + y_\chi\phi)^2. \quad (18d)$$

We adopt the $\overline{\text{MS}}$ scheme in this study and thus subsequently choose $\mu = v_S$. Further, the one-loop correction to the scalar potential induced due to $T \neq 0$ reads [71–73]

$$V_T(\phi, T) = \frac{T^4}{2\pi^2} \left[\sum_{b=\text{boson}} n_b J_B\left(\frac{M_b^2(\phi)}{T^2}\right) + \sum_{f=\text{fermion}} n_f J_F\left(\frac{M_f^2(\phi)}{T^2}\right) \right]. \quad (19)$$

In the above, the indices b and f respectively run over the bosonic and fermionic fields. The functions $J_{B,F}(x)$ read

$$J_{B,F}(x) = \int_0^\infty dx y^2 \log[1 \mp e^{-\sqrt{y^2+x}}]. \quad (20)$$

Further, infrared effects are included using the daisy resummation technique [74, 75]. In particular, the Arnold-Espinosa prescription [75] that contributes the following term:

$$V_{\text{Daisy}}(\phi, T) = -\frac{T}{12\pi} \sum_{b=\text{boson}} n_b \left[M_b^3(\phi, T) - M_b^3(\phi) \right], \quad (21)$$

where $M_b^2(\phi, T) = M_b^2(\phi) + \Pi_b(T)$ refers to the thermal mass of the b th boson. The Debye mass corrections $\Pi_b(T)$ for the considered setup are relegated to the Appendix. In all, the scalar potential finite temperature becomes

$$V_{\text{total}}(\phi, T) = V_0(\phi) + V_{\text{CW}}(\phi) + V_{\text{Daisy}}(\phi, T). \quad (22)$$

The scalar potential above admits coexisting minima that can be obtained through

$$\frac{\partial V_{\text{total}}}{\partial \phi} = 0, \quad (23a)$$

$$\frac{\partial^2 V_{\text{total}}}{\partial \phi^2} > 0. \quad (23b)$$

The two minima ϕ_f and ϕ_t (say) can be dubbed as the false and the true vacuum respectively. Such dynamics therefore opens up the possibility of a first order phase transition (FOPT). It also entails tunnelling from ϕ_f to ϕ_t whose probability per unit 4-volume is given by [76]

$$\Gamma(T) = T^4 \left(\frac{S_E}{2\pi T} \right)^{3/2} e^{-\frac{S_E}{T}}. \quad (24)$$

Here, S_E is the classical euclidean "bounce" action in 3-dimensions calculated as

$$S_E = 4\pi \int_0^\infty dr r^2 \left[\frac{1}{2} \left(\frac{d\phi}{dr} \right)^2 + V_{\text{total}}(\phi, T) \right]. \quad (25)$$

The scalar field ϕ is derived by solving the classical field equation

$$\frac{d^2 \phi}{dr^2} + \frac{2}{r} \frac{d\phi}{dr} - \frac{\partial V_{\text{total}}}{\partial \phi} = 0. \quad (26)$$

A critical temperature T_c is identified through

$$V_{\text{total}}(\phi_f(T_c), T_c) = V_{\text{total}}(\phi_t(T_c), T_c), \quad (27)$$

The bubble picture can be invoked to understand FOPT in analogy with the liquid-gas phase transition. In a sea of the false vacuum can be thought to be populated by bubbles containing the true vacuum. And the bubbles grow in size as tunnelling from ϕ_f to ϕ_t proceeds. There is ~ 1 bubble per unit Hubble volume at the nucleation temperature T_n typically defined as

$$\frac{S_E(T_n)}{T_n} = 140. \quad (28)$$

Gravitational waves in case of an FOPT are mainly generated through (a) bubble wall collisions [77–81], (b) sound waves [82–85], and (c) magneto-hydrodynamic (MHD) turbulence [86–90] in the plasma. We express below the corresponding contributions to the energy

	BM1	BM2
M_{η_R}	351.194 GeV	228.89 GeV
M_χ	602.952 GeV	618.55 GeV
y_χ	1.754	1.838
$\Omega_{\eta_R} h^2$	0.019	0.010
$\Omega_\chi h^2$	0.081	0.072
$\sigma_{\eta_R}^{\text{SI}}$	$6.936 \times 10^{-48} \text{ cm}^2$	$1.62 \times 10^{-47} \text{ cm}^2$
σ_χ^{SI}	$8.25 \times 10^{-50} \text{ cm}^2$	$8.67 \times 10^{-50} \text{ cm}^2$
T_c	263.784 GeV	380.746 GeV
$\frac{\phi_c}{T_c}$	1.491	2.018
T_n	236.2 GeV	284.2 GeV
α_n	1.23×10^{-2}	1.84×10^{-3}
β	2.219×10^3	1.025×10^3
v_b	0.660	0.611
$\frac{M_\chi^*}{T^*}$	3.805	4.505
F_χ	0.459	0.590
$\Omega_{\text{FB}} h^2 / \Omega_{\text{obs}} h^2$	16.67%	31.67%
Required c_χ	4.93×10^{-3}	7.29×10^{-3}

TABLE I: Benchmark parameter points and the corresponding predictions of GW amplitude and Fermi-ball contribution to DM.

density as a function of the GW frequency f [91–96].

$$\Omega_{\text{coll}} h^2 = 1.67 \times 10^{-5} \left(\frac{\beta}{H}\right)^{-2} \left(\frac{0.11 v_b^3}{0.42 + v_b^2}\right) \left(\frac{\kappa_c \alpha}{1 + \alpha}\right)^2 \left(\frac{100}{g_*}\right)^{\frac{1}{3}} \left(\frac{3.8(f/f_{\text{coll}})^{2.8}}{1 + 2.8(f/f_{\text{coll}})^{3.8}}\right), \quad (29\text{a})$$

$$\Omega_{\text{sw}} h^2 = 2.65 \times 10^{-6} \left(\frac{\beta}{H}\right)^{-1} v_b \left(\frac{\kappa_s \alpha}{1 + \alpha}\right)^2 \left(\frac{100}{g_*}\right)^{\frac{1}{3}} \left(\frac{f}{f_{\text{sw}}}\right)^3 \left(\frac{7}{4 + 3(f/f_{\text{sw}})^2}\right)^{7/2}, \quad (29\text{b})$$

$$\Omega_{\text{tur}} h^2 = 3.35 \times 10^{-4} \left(\frac{\beta}{H}\right)^{-1} v_b \left(\frac{\kappa_t \alpha}{1 + \alpha}\right)^{3/2} \left(\frac{100}{g_*}\right)^{\frac{1}{3}} \left(\frac{f}{f_{\text{tur}}}\right)^3 \frac{(1 + f/f_{\text{tur}})^{-11/3}}{1 + 8\pi f/h_s}. \quad (29\text{c})$$

In the above, the parameter α [97] is defined as

$$\alpha = \frac{\Delta\rho}{\rho_r(T_n)}, \quad (30)$$

where $\Delta\rho =$

$\left[V_{\text{total}}(\phi_f(T), T) - V_{\text{total}}(\phi_t(T), T) - T \frac{d}{dT} (V_{\text{total}}(\phi_f(T), T) - V_{\text{total}}(\phi_t(T), T)) \right]_{T=T_n}$ parameterizes the energy budget of the FOPT through its latent heat release. Moreover, $\rho_r(T) = \frac{\pi^2}{30} g_* T^4$ is the energy density of the radiation dominated phase in the presence

of g_* number of relativistic degrees of freedom. One also has

$$\beta = T_n \left. \frac{dS_E}{dT} \right|_{T=T_n} \quad (31)$$

[98] that quantifies the speed of phase transition. Further, v_b is the bubble wall velocity in general related to the Jouget velocity $v_J = \frac{1/\sqrt{3} + \sqrt{\alpha^2 + 2\alpha/3}}{1+\alpha}$ [94–96]. One reckons $v_b \simeq v_J$ unless there is supercooling. The factors κ_c, κ_s and κ_t respectively are efficiency factors relevant to bubble collision, sound wave emission and turbulence. They are expressed as

$$\kappa_c = \frac{1}{1 + 0.715\alpha} \left(0.715\alpha + \frac{4}{27} \sqrt{\frac{3\alpha}{2}} \right), \quad (32a)$$

$$\kappa_s = \frac{\sqrt{\alpha}}{0.135 + \sqrt{0.98 + \alpha}}, \quad (32b)$$

$$\kappa_t = 0.1\kappa_s. \quad (32c)$$

Finally, the frequencies f_{coll} , f_{sw} and f_{turb} at which the corresponding GW amplitudes peak [91–96] are expressed below.

$$f_{coll} = 1.65 \times 10^{-5} \text{Hz} \left(\frac{g_*}{100} \right)^{1/6} \left(\frac{T_n}{100 \text{ GeV}} \right) \left(\frac{0.62}{v_b^2 - 0.1v_b + 1.8} \right) \left(\frac{\beta}{H} \right), \quad (33a)$$

$$f_{sw} = 1.65 \times 10^{-5} \text{Hz} \left(\frac{g_*}{100} \right)^{1/6} \left(\frac{T_n}{100 \text{ GeV}} \right) \left(\frac{2}{\sqrt{3}} \right) \left(\frac{\beta}{H} \right), \quad (33b)$$

$$f_{tur} = 1.65 \times 10^{-5} \text{Hz} \left(\frac{g_*}{100} \right)^{1/6} \left(\frac{T_n}{100 \text{ GeV}} \right) \left(\frac{7}{4} \right) \left(\frac{\beta}{H} \right). \quad (33c)$$

The total GW density is therefore the sum of the individual contributions from bubble collision, sound wave production and turbulence. Thus,

$$\Omega_{\text{GW}} h^2 = \Omega_{\text{coll}} h^2 + \Omega_{\text{sw}} h^2 + \Omega_{\text{tur}} h^2. \quad (34)$$

We fix $M_H = v_S = \mu_S = 200 \text{ GeV}$, $\lambda_L = 0.01$, $s_\theta = 5 \times 10^{-4}$, $y_\chi = 1.8$, $\lambda_7 = 1, 2$ for illustration and make the following variation $100 \text{ GeV} \leq M_{\eta_R}, M_\chi \leq 1 \text{ TeV}$ in our numerical scans. The scan range is motivated from the fact that we wish to probe the IDM desert region in terms of the GW spectrum and Fermi-ball formation. The parameter regions in the $M_{\eta_R} - M_\chi$ plane corresponding to $\frac{\phi_c}{T_c} > 1, 2, 3$ are overlaid on the region accounting for $\geq 50\%$ of the observed relic abundance in Fig.3. An FOPT with $\frac{\phi_c}{T_c} \geq 1$ is dubbed *strong* hereafter. The results of Fig.3 demonstrate the possibility of accommodating together a strong FOPT and an elevated thermal relic abundance in the IDM desert region. This point emerges as a major upshot of this study. We would like to mention that the wide [0.06,0.12] interval for the thermal relic is chosen deliberately in order to leave room for a possible Fermi-ball contribution.

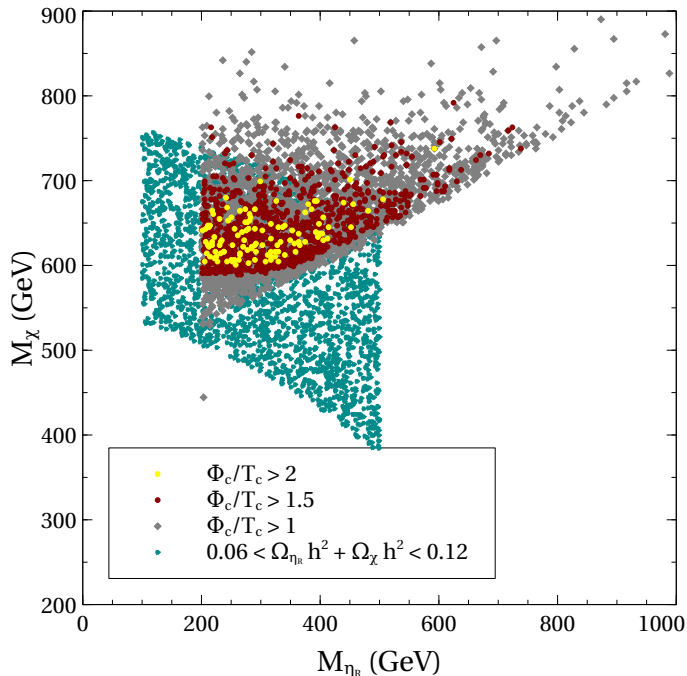


FIG. 3: Variation of $V_{\text{total}}(\phi, T)$ versus ϕ for $T = T_c, T_n$ in case of BP1 and BP2. The color coding is explained in the legends.

To advance the discussion further, we pick two two representative benchmarks from the desert region that predict strong FOPT. The benchmarks, BM1 and BM2, are displayed in in Table I. The shape of $V_{\text{total}}(\phi, T)$ is shown at the critical and nucleation temperatures for the chosen benchmarks in Fig.4.

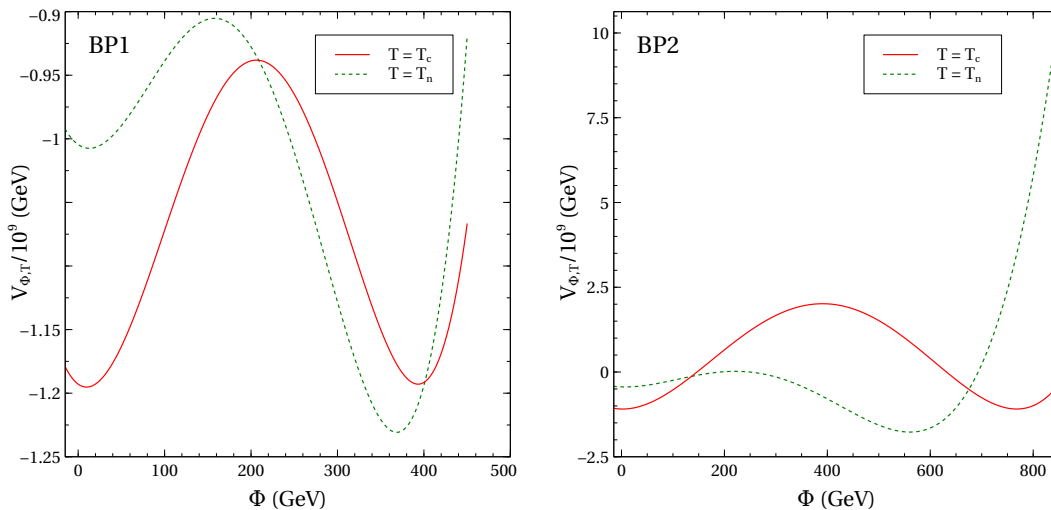


FIG. 4: Regions in the $M_{\eta_R} - M_\chi$ plane simultaneously accounting for strong FOPT and at least 50% of the observed DM relic. The color coding is explained in the legends.

The WIMP DM density for both benchmarks is majorly generated by the fermion χ though the IDM shares $\gtrsim 15\%$ of the WIMP contribution. The corresponding S_E at various T are computed using the publicly available tool `FindBounce` [99]. The parameters relevant to an $\Omega_{\text{GW}}h^2$ calculation are also shown in the table. The GW spectra corresponding to these benchmarks can be seen in Fig.5. The GW spectra peak at around $\mathcal{O}(10^{-15})$ and $\mathcal{O}(10^{-17})$ values for BM1 and BM2 respectively. And the shapes of the spectra are such that BM1 is within the reach of the proposed GW detector BBO [100]. BM2 can also be probed by the U-DECIGO detector [101, 102]. Given the representative nature of the chosen benchmarks, it is inferred that the IDM desert region can be probed by the aforementioned experiments.

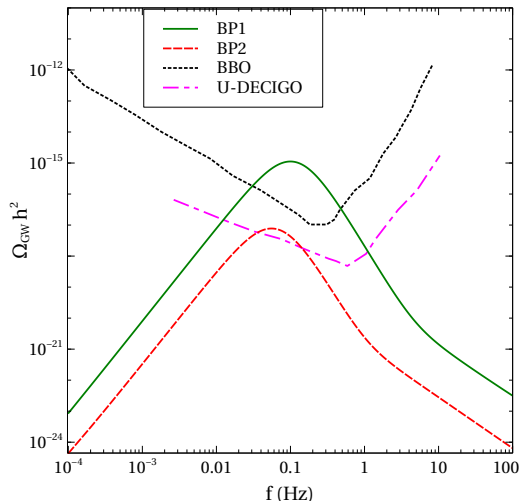


FIG. 5: Variation of $V_{\text{total}}(\phi, T)$ versus ϕ for $T = T_c, T_n$ in case of BP1 and BP2. The color coding is explained in the legends.

The possibility of Fermi-ball formation in this specific framework is discussed next. We first define $\Delta U(T) = V_{\text{total}}(\phi_f(T), T) - V_{\text{total}}(\phi_t(T), T)$. The energy of a Fermi-ball for $T \simeq 0$ with global charge Q_{FB} and radius R reads

$$E = \frac{3\pi}{4} \left(\frac{3}{2\pi} \right)^{2/3} \frac{Q_{\text{FB}}^{4/3}}{R} + 4\pi\sigma_0 R^2 + \frac{4\pi}{3} U_0 R^3. \quad (35)$$

where the first term is the Fermi-gas pressure of χ , σ_0 the surface tension, and $U_0 = \Delta U(T)|_{T=0}$. The surface term can be neglected compared to the volume term given the macroscopic size of the Fermi-balls. Following closely the analysis of [50], we find that stability of the a Fermi-ball requires

$$(12\pi^2 U_0)^{1/4} < m_\chi + y_\chi \phi_t(0). \quad (36)$$

The expressions for the mass, radius and charge of a Fermi-ball can be found in [50] and are therefore skipped here. It is clear that Fermi-ball formation necessitates coexisting minima of the scalar potential at zero temperature. This can be arranged through the trilinear $-\frac{1}{3}\mu_S\phi^3$ term. Thus, in retrospect, the introduction of such a term stands justified.

A important quantity in the context of Fermi-balls is the fraction of χ trapped in the false vacuum. Denoting the same by F_χ , it can be obtained as a function of the bubble wall velocity v_b and M_χ^*/T_* . Here, T_* refers to the temperature where Fermi-balls start to form and M_χ^* is the field dependent mass of the fermion at that temperature. We take $T_* \simeq T_n$ in this analysis, an approximation that remains valid for a non-supercooled FOPT such as the ones under consideration. Finally, Fermi-balls contribute to the relic density by

$$\Omega_{\text{FB}}h^2 = 0.12 \times F_\chi \left(\frac{c_\chi}{0.0146} \right) \left(\frac{U_0^{1/4}}{100 \text{ GeV}} \right), \quad (37)$$

where c_χ is a number typically ~ 0.01 . The observed relic is thus a sum of the contributions from DM scattering and Fermi-balls. That is,

$$\Omega_{\text{obs}}h^2 = \Omega_{\eta_R}h^2 + \Omega_\chi h^2 + \Omega_{\text{FB}}h^2. \quad (38)$$

The values of F_χ and the relative contributions of Fermi-balls to the observed relic density are shown in Table I. It is seen that the contributions are sizeable and exceed the contribution from η . In fact, Fermi-balls account for $\simeq 32\%$ of the observed DM for BP2. In the last row of the same table, we also estimate the value of c_χ stipulated in the process.

V. SUMMARY

We have revisited a two-component DM model involving an inert scalar η and a fermion χ that are respectively doublet and singlet under $SU(2)_L$. The fermion interacts with the rest of the fields through an $SU(2)_L$ scalar S , and, makes up for the relic density in regions where the standalone inert doublet would lead to under-abundance. This is particularly true for the 100 - 500 GeV mass range of the inert doublet where we focus on in this study.

The presence of a cubic term in the scalar potential leads to co-existing minima. This possibility is enhanced by $T \neq 0$ corrections thereby triggering first order phase transitions. We have demonstrated in this study that the aforementioned mass range of the inert doublet can lead to a *strong* FOPT for appropriate values of the other parameters. Two representative benchmarks are chosen with T_n in the 200-300 GeV range. The gravitational wave spectrum arising out of FOPT is also looked at. We obtain $\Omega_{\text{GW}}h^2 \simeq \mathcal{O}(10^{-17})$ for frequency $\sim \mathcal{O}(0.1)$ Hz implying that the proposed benchmarks can be probed by the proposed BBO and U-DECIGO GW detectors.

We have also shown that the present scenario allows for the formation of stable Fermi-balls in the parameter region sensitive to the aforesaid detectors in terms of the strength of GW production. The contribution of Fermi-balls to DM relic density is also estimated. It is seen that the Fermi-ball contribution can be a sizeable $\gtrsim 30\%$ of the observed relic density.

Acknowledgement

IC acknowledges support from Department of Science and Technology, Govt. of India, under grant number IFA18-PH214 (INSPIRE Faculty Award). NC acknowledges support from Department of Science and Technology, Govt. of India, under grant number IFA19-PH237 (INSPIRE Faculty Award). HR is supported by the National Natural Science Foundation of China under Grant Nos. 12475094, 12135006 and 12075097, as well as by the Fundamental Research Funds for the Central Universities under Grant No. CCNU24AI003.

VI. APPENDIX

A. Model couplings

$$y_{h\chi\chi} = -y_{\chi} s_{\theta}, \quad (39a)$$

$$y_{H\chi\chi} = y_{\chi} c_{\theta}, \quad (39b)$$

$$\lambda_{h\eta_R\eta_R} = \lambda_L v c_{\theta} - \lambda_7 v_S s_{\theta}, \quad (39c)$$

$$\lambda_{h\eta_I\eta_I} = (\lambda_3 + \lambda_4 - \lambda_5) v c_{\theta} - \lambda_7 v_S s_{\theta}, \quad (39d)$$

$$\lambda_{h\eta^+\eta^-} = \lambda_3 v c_{\theta} - \lambda_7 v_S s_{\theta}, \quad (39e)$$

$$\lambda_{H\eta_R\eta_R} = \lambda_L v s_{\theta} + \lambda_7 v_S c_{\theta}, \quad (39f)$$

$$\lambda_{H\eta_I\eta_I} = (\lambda_3 + \lambda_4 - \lambda_5) v s_{\theta} + \lambda_7 v_S c_{\theta}, \quad (39g)$$

$$\lambda_{H\eta^+\eta^-} = \lambda_3 v s_{\theta} + \lambda_7 v_S c_{\theta}. \quad (39h)$$

B. Debye mass corrections

$$\Pi_{h_0}(T) = \frac{1}{12} \left(6\lambda_1 + 2\lambda_3 + \lambda_4 + \frac{1}{2}\lambda_6 + \frac{3}{4}(g')^2 + \frac{9}{4}g^2 + 3y_t^2 \right) T^2, \quad (40a)$$

$$\Pi_{G_0}(T) = \Pi_{G^+}(T) = \Pi_{h_0}(T), \quad (40b)$$

$$\Pi_{\eta_R}(T) = \frac{1}{12} \left(6\lambda_2 + 2\lambda_3 + \lambda_4 + \frac{1}{2}\lambda_7 + \frac{3}{4}(g')^2 + \frac{9}{4}g^2 \right) T^2, \quad (40c)$$

$$\Pi_{\eta_I}(T) = \Pi_{\eta^+}(T) = \Pi_{\eta_R}(T), \quad (40d)$$

$$\Pi_{s_0}(T) = \left(2\lambda_6 + 2\lambda_7 + 3\lambda_8 + 2y_\chi^2 \right) \frac{T^2}{12}. \quad (40e)$$

- [1] W. Collaboration, *Wilkinson microwave anisotropy probe (wmap) three year results: Implications for cosmology*, *Astrophys. J. Suppl.* **170** (2007) 377, [[astro-ph/0603449](#)].
- [2] P. Collaboration, *Planck 2018 results. vi. cosmological parameters*, [arXiv:1807.06209](#).
- [3] N. A. et al. (Planck Collaboration), *Planck 2018 results. vi. cosmological parameters*, *Astron. Astrophys.* **641** (2020) A6.
- [4] G. Bertone, D. Hooper and J. Silk, *Particle dark matter: Evidence, candidates and constraints*, *Phys. Rep.* **405** (2005) 279.
- [5] B. W. Lee and S. Weinberg, *Cosmological lower bound on heavy-neutrino masses*, *Phys. Rev. Lett.* **39** (1977) 165.
- [6] L. Collaboration, *Results from a search for dark matter in the complete lux exposure*, *Phys. Rev. Lett.* **118** (2017) 021303, [[arXiv:1608.07648](#)].
- [7] P. Collaboration, *Dark matter direct search sensitivity of the pandax-4t experiment*, *Sci. China Phys. Mech. Astron.* **62** (2019) 31011, [[arXiv:1806.02229](#)].
- [8] X. Collaboration, *Dark matter search results from a one tonyear exposure of xenon1t*, *Phys. Rev. Lett.* **121** (2018) 111302, [[arXiv:1805.12562](#)].
- [9] C. Amole, M. Ardid, I. J. Arnquist, D. M. Asner, D. Baxter, E. Behnke et al., *Dark matter search results from the complete exposure of the pico-60 c₃f₈ bubble chamber*, *Phys. Rev. D* **100** (2019) 022001, [[arXiv:1902.04031](#)].
- [10] S. Bhattacharya, A. Drozd, B. Grzadkowski and J. Wudka, *Two-component dark matter*, *JHEP* **10** (2013) 158, [[arXiv:1309.2986](#)].
- [11] L. Bian, R. Ding and B. Zhu, *Two component higgs-portal dark matter*, *Phys. Lett. B* **728** (2014) 105, [[arXiv:1308.3851](#)].
- [12] S. Esch, M. Klasen and C. E. Yaguna, *A minimal model for two-component dark matter*, *JHEP* **09** (2014) 108, [[arXiv:1406.0617](#)].

- [13] S. Bhattacharya, P. Poulouze and P. Ghosh, *Multipartite interacting scalar dark matter in the light of updated lux data*, *JCAP* **04** (2017) 043, [[arXiv:1607.08461](#)].
- [14] A. Ahmed, M. Duch, B. Grzadkowski and M. Iglicki, *Multi-component dark matter: the vector and fermion case*, *Eur. Phys. J. C* **78** (2018) 905, [[arXiv:1710.01853](#)].
- [15] J. Herrero-Garcia, A. Scaffidi, M. White and A. G. Williams, *On the direct detection of multi-component dark matter: sensitivity studies and parameter estimation*, *JCAP* **11** (2017) 021, [[arXiv:1709.01945](#)].
- [16] J. Herrero-Garcia, A. Scaffidi, M. White and A. G. Williams, *On the direct detection of multi-component dark matter: implications of the relic abundance*, *JCAP* **01** (2019) 008, [[arXiv:1809.06881](#)].
- [17] A. Poulin and S. Godfrey, *Multicomponent dark matter from a hidden gauged $su(3)$* , *Phys. Rev. D* **99** (2019) 076008, [[arXiv:1808.04901](#)].
- [18] M. Aoki and T. Toma, *Boosted self-interacting dark matter in a multi-component dark matter model*, *JCAP* **10** (2018) 020, [[arXiv:1806.09154](#)].
- [19] M. Aoki, D. Kaneko and J. Kubo, *Multicomponent dark matter in radiative seesaw models*, *Front. Phys.* **5** (2017) 53, [[arXiv:1711.03765](#)].
- [20] F. Elahi and S. Khatibi, *Multi-component dark matter in a non-abelian dark sector*, *Phys. Rev. D* **100** (2019) 015019, [[arXiv:1902.04384](#)].
- [21] D. Borah, R. Roshan and A. Sil, *Minimal two-component scalar doublet dark matter with radiative neutrino mass*, *Phys. Rev. D* **100** (2019) 055027, [[arXiv:1904.04837](#)].
- [22] S. Bhattacharya, P. Ghosh, A. K. Saha and A. Sil, *Two component dark matter with inert higgs doublet: neutrino mass, high scale validity and collider searches*, *JHEP* **03** (2020) 090, [[arXiv:1905.12583](#)].
- [23] S. Bhattacharya, N. Chakrabarty, R. Roshan and A. Sil, *Multicomponent dark matter in extended $U(1)$ $B-L$: neutrino mass and high scale validity*, *JCAP* **04** (2020) 013, [[1910.00612](#)].
- [24] N. Chakrabarty, R. Roshan and A. Sil, *Two-component doublet-triplet scalar dark matter stabilizing the electroweak vacuum*, *Phys. Rev. D* **105** (2022) 115010, [[2102.06032](#)].
- [25] N. Blinov, S. Profumo and T. Stefaniak, *The Electroweak Phase Transition in the Inert Doublet Model*, *JCAP* **07** (2015) 028, [[1504.05949](#)].
- [26] S. Jangid and H. Okada, *Electroweak phase transition with radiative symmetry breaking in a type-II seesaw model with an inert doublet*, *Phys. Rev. D* **109** (2024) 015001, [[2310.12591](#)].
- [27] P. Bandyopadhyay and S. Jangid, *Discerning singlet and triplet scalars at the electroweak phase transition and gravitational wave*, *Phys. Rev. D* **107** (2023) 055032, [[2111.03866](#)].
- [28] N. Chakrabarty, H. Roy and T. Srivastava, *Single-step first order phase transition and*

- gravitational waves in a SIMP dark matter scenario*, *Nucl. Phys. B* **998** (2024) 116392, [[2212.09659](#)].
- [29] L. Bian, Y.-L. Tang and R. Zhou, *FIMP dark matter mediated by a massive gauge boson around the phase transition period and the gravitational waves production*, *Phys. Rev. D* **106** (2022) 035028, [[2111.10608](#)].
- [30] X. Deng, X. Liu, J. Yang, R. Zhou and L. Bian, *Heavy dark matter and Gravitational waves*, *Phys. Rev. D* **103** (2021) 055013, [[2012.15174](#)].
- [31] L. Bian and X. Liu, *Two-step strongly first-order electroweak phase transition modified FIMP dark matter, gravitational wave signals, and the neutrino mass*, *Phys. Rev. D* **99** (2019) 055003, [[1811.03279](#)].
- [32] F. Costa, S. Khan and J. Kim, *A two-component dark matter model and its associated gravitational waves*, *JHEP* **06** (2022) 026, [[2202.13126](#)].
- [33] P. Ghosh, T. Ghosh and S. Roy, *Interplay among gravitational waves, dark matter and collider signals in the singlet scalar extended type-II seesaw model*, *JHEP* **10** (2023) 057, [[2211.15640](#)].
- [34] A. Chatterjee, A. Datta and S. Roy, *Electroweak phase transition in the Z_3 -invariant NMSSM: Implications of LHC and Dark matter searches and prospects of detecting the gravitational waves*, *JHEP* **06** (2022) 108, [[2202.12476](#)].
- [35] T. Ghosh, H.-K. Guo, T. Han and H. Liu, *Electroweak phase transition with an $SU(2)$ dark sector*, *JHEP* **07** (2021) 045, [[2012.09758](#)].
- [36] H. Shibuya and T. Toma, *Impact of first-order phase transitions on dark matter production in the scotogenic model*, *JHEP* **11** (2022) 064, [[2207.14662](#)].
- [37] A. Addazi and A. Marcianò, *Gravitational waves from dark first order phase transitions and dark photons**, *Chinese Physics C* **42** (jan, 2018) 023107.
- [38] N. Benincasa, A. Hryczuk, K. Kannike and M. Laletin, *Phase transitions and gravitational waves in a model of \mathbb{Z}_3 scalar dark matter*, *JHEP* **02** (2024) 207, [[2312.04627](#)].
- [39] R. Allahverdi, C. Hauptmann and P. Huang, *Enhanced dark matter abundance in first-order phase transitions*, *Phys. Rev. D* **110** (2024) 115005, [[2409.02179](#)].
- [40] I. K. Banerjee, U. K. Dey and S. Khalil, *Primordial Black Holes and Gravitational Waves in the $U(1)$ B - L extended inert doublet model: a first-order phase transition perspective*, *JHEP* **12** (2024) 009, [[2406.12518](#)].
- [41] S. Biondini, P. Schicho and T. V. I. Tenkanen, *Strong electroweak phase transition in t -channel simplified dark matter models*, *JCAP* **10** (2022) 044, [[2207.12207](#)].
- [42] D. Borah, S. Jyoti Das and I. Saha, *Dark matter from phase transition generated PBH evaporation with gravitational waves signatures*, *Phys. Rev. D* **110** (2024) 035014,

- [2401.12282].
- [43] D. Borah, A. Dasgupta, M. Knauss and I. Saha, *Baryon asymmetry from dark matter decay in the vicinity of a phase transition*, *Phys. Rev. D* **108** (2023) L091701, [2306.05459].
- [44] D. Borah, A. Dasgupta and I. Saha, *Ligo-virgo constraints on dark matter and leptogenesis triggered by a first order phase transition at high scale*, *Phys. Rev. D* **109** (May, 2024) 095034.
- [45] D. Borah, A. Dasgupta and I. Saha, *Leptogenesis and dark matter through relativistic bubble walls with observable gravitational waves*, *JHEP* **11** (2022) 136, [2207.14226].
- [46] D. Borah, S. Jyoti Das and R. Roshan, *Probing high scale seesaw and PBH generated dark matter via gravitational waves with multiple tilts*, *Nucl. Phys. B* **1002** (2024) 116528, [2208.04965].
- [47] D. Borah, A. Dasgupta and S. K. Kang, *A first order dark $SU(2)_D$ phase transition with vector dark matter in the light of NANOGrav 12.5 yr data*, *JCAP* **12** (2021) 039, [2109.11558].
- [48] D. Borah, A. Dasgupta and S. K. Kang, *Gravitational waves from a dark $U(1)_D$ phase transition in light of NANOGrav 12.5 yr data*, *Phys. Rev. D* **104** (2021) 063501, [2105.01007].
- [49] X. Liu and L. Bian, *Dark matter and electroweak phase transition in the mixed scalar dark matter model*, *Phys. Rev. D* **97** (2018) 055028, [1706.06042].
- [50] J.-P. Hong, S. Jung and K.-P. Xie, *Fermi-ball dark matter from a first-order phase transition*, *Phys. Rev. D* **102** (2020) 075028, [2008.04430].
- [51] A. Belyaev, G. Cacciapaglia, I. P. Ivanov, F. Rojas-Abatte and M. Thomas, *Anatomy of the inert two higgs doublet model in the light of the lhc and non-lhc dark matter searches*, *Physical Review D* **97** (2018) 035011, [arXiv:1612.00511].
- [52] L. L. Honorez, E. Nezri, J. F. Oliver and M. H. G. Tytgat, *The inert doublet model: an archetype for dark matter*, *Journal of Cosmology and Astroparticle Physics* **02** (2007) 028, [hep-ph/0612275].
- [53] L. L. Honorez and C. E. Yaguna, *The inert doublet model of dark matter revisited*, *Journal of High Energy Physics* **09** (2010) 046, [arXiv:1003.3125].
- [54] A. Arhrib, Y.-L. S. Tsai, Q. Yuan and T.-C. Yuan, *An updated analysis of inert higgs doublet model in light of the recent results from lux, planck, ams-02 and lhc*, *Journal of Cosmology and Astroparticle Physics* **06** (2014) 030, [arXiv:1310.0358].
- [55] S. Choubey and A. Kumar, *Inflation and dark matter in the inert doublet model*, *Journal of High Energy Physics* **11** (2017) 080, [arXiv:1707.06587].
- [56] L. L. Honorez and C. E. Yaguna, *A new viable region of the inert doublet model*, *Journal of*

- Cosmology and Astroparticle Physics* **01** (2011) 002, [[arXiv:1011.1411](#)].
- [57] A. Ilnicka, M. Krawczyk and T. Robens, *Inert doublet model in light of lhc run i and astrophysical data*, *Physical Review D* **93** (2016) 055026, [[arXiv:1508.01671](#)].
- [58] Q.-H. Cao, E. Ma and G. Rajasekaran, *Observing the dark scalar doublet and its impact on the standard-model higgs boson at colliders*, *Physical Review D* **76** (2007) 095011, [[arXiv:0708.2939](#)].
- [59] E. Lundstrom, M. Gustafsson and J. Edsjo, *The inert doublet model and lep ii limits*, *Physical Review D* **79** (2009) 035013, [[arXiv:0810.3924](#)].
- [60] M. Gustafsson, S. Rydbeck, L. Lopez-Honorez and E. Lundstrom, *Status of the inert doublet model and the role of multileptons at the lhc*, *Physical Review D* **86** (2012) 075019, [[arXiv:1206.6316](#)].
- [61] J. Kalinowski, W. Kotlarski, T. Robens, D. Sokolowska and A. F. Zarnecki, *Benchmarking the inert doublet model for $e + e -$ colliders*, *Journal of High Energy Physics* **12** (2018) 081, [[arXiv:1809.07712](#)].
- [62] S. Chakraborti and P. Poulose, *Interplay of Scalar and Fermionic Components in a Multi-component Dark Matter Scenario*, *Eur. Phys. J. C* **79** (2019) 420, [[1808.01979](#)].
- [63] E. W. Kolb, *The Early Universe*, vol. 69. Taylor and Francis, 5, 2019, [10.1201/9780429492860](#).
- [64] A. Semenov, *LanHEP: A Package for the automatic generation of Feynman rules in field theory. Version 3.0*, *Comput. Phys. Commun.* **180** (2009) 431–454, [[0805.0555](#)].
- [65] G. Belanger, F. Boudjema, A. Pukhov and A. Semenov, *micrOMEGAs4.1: two dark matter candidates*, *Comput. Phys. Commun.* **192** (2015) 322–329, [[1407.6129](#)].
- [66] LUX collaboration, D. S. Akerib et al., *Results from a search for dark matter in the complete LUX exposure*, *Phys. Rev. Lett.* **118** (2017) 021303, [[1608.07648](#)].
- [67] PANDAX-II collaboration, X. Cui et al., *Dark Matter Results From 54-Ton-Day Exposure of PandaX-II Experiment*, *Phys. Rev. Lett.* **119** (2017) 181302, [[1708.06917](#)].
- [68] XENON collaboration, E. Aprile et al., *Dark Matter Search Results from a One Tonyear Exposure of XENON1T*, *Phys. Rev. Lett.* **121** (2018) 111302, [[1805.12562](#)].
- [69] J. M. Alarcon, L. S. Geng, J. Martin Camalich and J. A. Oller, *The strangeness content of the nucleon from effective field theory and phenomenology*, *Phys. Lett. B* **730** (2014) 342–346, [[1209.2870](#)].
- [70] S. R. Coleman and E. J. Weinberg, *Radiative corrections as the origin of spontaneous symmetry breaking*, *Physical Review D* **7** (1973) 1888–1910.
- [71] L. Dolan and R. Jackiw, *Symmetry behavior at finite temperature*, *Physical Review D* **9** (1974) 3320–3341.

- [72] M. Quiros, *Finite temperature field theory and phase transitions*, in *ICTP Summer School in High-Energy Physics and Cosmology*, pp. 187–259, 1, 1999. [hep-ph/9901312](#).
- [73] M. Laine and A. Vuorinen, *Basics of Thermal Field Theory*, vol. 925. Springer, 2016, [10.1007/978-3-319-31933-9](#).
- [74] R. R. Parwani, *Resummation in a hot scalar field theory*, *Physical Review D* **45** (1992) 4695, [[hep-ph/9204216](#)].
- [75] P. B. Arnold and O. Espinosa, *The effective potential and first order phase transitions: Beyond leading-order*, *Physical Review D* **47** (1993) 3546, [[hep-ph/9212235](#)].
- [76] A. D. Linde, *Decay of the false vacuum at finite temperature*, *Nuclear Physics B* **216** (1983) 421.
- [77] M. S. Turner and F. Wilczek, *Relic gravitational waves and extended inflation*, *Physical Review Letters* **65** (1990) 3080–3083.
- [78] A. Kosowsky, M. S. Turner and R. Watkins, *Gravitational radiation from colliding vacuum bubbles*, *Phys. Rev. D* **45** (1992) 4514–4535.
- [79] A. Kosowsky, M. S. Turner and R. Watkins, *Gravitational waves from first order cosmological phase transitions*, *Phys. Rev. Lett.* **69** (1992) 2026–2029.
- [80] A. Kosowsky and M. S. Turner, *Gravitational radiation from colliding vacuum bubbles: envelope approximation to many bubble collisions*, *Physical Review D* **47** (1993) 4372–4391, [[astro-ph/9211004](#)].
- [81] M. S. Turner, E. J. Weinberg and L. M. Widrow, *Bubble nucleation in first-order inflation and other cosmological phase transitions*, *Phys. Rev. D* **46** (Sep, 1992) 2384–2403.
- [82] M. Hindmarsh, S. J. Huber, K. Rummukainen and D. J. Weir, *Gravitational waves from the sound of a first order phase transition*, *Phys. Rev. Lett.* **112** (2014) 041301, [[1304.2433](#)].
- [83] J. T. Giblin and J. B. Mertens, *Gravitational radiation from first-order phase transitions in the presence of a fluid*, *Physical Review D* **90** (2014) 023532, [[1405.4005](#)].
- [84] M. Hindmarsh, S. J. Huber, K. Rummukainen and D. J. Weir, *Numerical simulations of acoustically generated gravitational waves at a first order phase transition*, *Phys. Rev. D* **92** (2015) 123009, [[1504.03291](#)].
- [85] M. Hindmarsh, S. J. Huber, K. Rummukainen and D. J. Weir, *Shape of the acoustic gravitational wave power spectrum from a first order phase transition*, *Phys. Rev. D* **96** (2017) 103520, [[1704.05871](#)].
- [86] A. Kosowsky, A. Mack and T. Kahniashvili, *Gravitational radiation from cosmological turbulence*, *Phys. Rev. D* **66** (2002) 024030, [[astro-ph/0111483](#)].
- [87] C. Caprini and R. Durrer, *Gravitational waves from stochastic relativistic sources: Primordial turbulence and magnetic fields*, *Phys. Rev. D* **74** (2006) 063521,

- [[astro-ph/0603476](#)].
- [88] G. Gogoberidze, T. Kahniashvili and A. Kosowsky, *The spectrum of gravitational radiation from primordial turbulence*, *Phys. Rev. D* **76** (2007) 083002, [[arXiv:0705.1733](#)].
- [89] C. Caprini, R. Durrer and G. Servant, *The stochastic gravitational wave background from turbulence and magnetic fields generated by a first-order phase transition*, *JCAP* **12** (2009) 024, [[arXiv:0909.0622](#)].
- [90] P. Niksa, M. Schlexer and G. Sigl, *Gravitational waves produced by compressible mhd turbulence from cosmological phase transitions*, *Class. Quant. Grav.* **35** (2018) 144001, [[arXiv:1803.02271](#)].
- [91] C. Caprini et al., *Science with the space-based interferometer elisa. ii: Gravitational waves from cosmological phase transitions*, *JCAP* **04** (2016) 001, [[arXiv:1512.06239](#)].
- [92] H.-K. Guo, K. Sinha, D. Vagie and G. White, *Phase transitions in an expanding universe: Stochastic gravitational waves in standard and non-standard histories*, *JCAP* **01** (2021) 001, [[arXiv:2007.08537](#)].
- [93] C. Caprini et al., *Detecting gravitational waves from cosmological phase transitions with lisa: an update*, *JCAP* **03** (2020) 024, [[arXiv:1910.13125](#)].
- [94] M. Kamionkowski, A. Kosowsky and M. S. Turner, *Gravitational radiation from first order phase transitions*, *Phys. Rev. D* **49** (1994) 2837–2851, [[astro-ph/9310044](#)].
- [95] P. J. Steinhardt, *Relativistic detonation waves and bubble growth in false vacuum decay*, *Phys. Rev. D* **25** (1982) 2074.
- [96] J. R. Espinosa, T. Konstandin, J. M. No and G. Servant, *Energy budget of cosmological first-order phase transitions*, *JCAP* **06** (2010) 028, [[arXiv:1004.4187](#)].
- [97] M. Kamionkowski, A. Kosowsky and M. S. Turner, *Gravitational radiation from first order phase transitions*, *Physical Review D* **49** (1994) 2837, [[astro-ph/9310044](#)].
- [98] A. Nicolis, *Relic gravitational waves from colliding bubbles and cosmic turbulence*, *Classical and Quantum Gravity* **21** (2004) L27, [[gr-qc/0303084](#)].
- [99] V. Guada, M. Nemevsek and M. Pintar, *FindBounce: Package for multi-field bounce actions*, *Comput. Phys. Commun.* **256** (2020) 107480, [[2002.00881](#)].
- [100] K. Yagi and N. Seto, *Detector configuration of decigo/bbo and identification of cosmological neutron-star binaries*, *Physical Review D* **83** (2011) 044011, [[1101.3940](#)].
- [101] S. S. et al., *The status of decigo*, *Journal of Physics: Conference Series* **840** (2017) 012010.
- [102] T. I. et al., *Improvement of the target sensitivity in decigo by optimizing its parameters for quantum noise including the effect of diffraction loss*, *Galaxies* **9** (2021) 14, [[2012.11859](#)].